Segmentation of 4D cardiac computed tomography images using active shape models

Leiner Barba-J[a], Jimena Olveres[a], Boris Escalante-Ramírez[a],
Fernando Arámbula[b], Enrique Vallejo[c]
[a]Dep. de Procesamiento de Señales, Facultad de Ingeniería; [b]Centro de Ciencias Aplicadas y Desarrollo Tecnológico, Universidad Nacional Autónoma de México, [c]Instituto Nacional de Cardiología, Ciudad de México

ABSTRACT

This paper describes a segmentation method for time series of 3D cardiac images based on deformable models. The goal of this work is to extend active shape models (ASM) of tree-dimensional objects to the problem of 4D (3D + time) cardiac CT image modeling. The segmentation is achieved by constructing a point distribution model (PDM) that encodes the spatio-temporal variability of a training set, i.e., the principal modes of variation of the temporal shapes are computed using some statistical parameters. An active search is used in the segmentation process where an initial approximation of the spatio-temporal shape is given and the gray level information in the neighborhood of the landmarks is analyzed. The starting shape is able to deform so as to better fit the data, but in the range allowed by the point distribution model. Several time series consisting of eleven 3D images of cardiac CT are employed for the method validation. Results are compared with manual segmentation made by an expert. The proposed application can be used for clinical evaluation of the left ventricle mechanical function. Likewise, the results can be taken as the first step of processing for optic flow estimation algorithms.

Keywords: Active shape models, image segmentation, 4D cardiac CT images

1. INTRODUCTION

Cardiac computed tomography is one of the main types of radiological images for heart analysis and detection of abnormalities. It provides image slices or tomograms of the heart[1] that form a tridimensional object. Since the heart is an organ with a periodic movement, analysis with cardiac CT can be made in 4D as well, which consists of several 3D images taken to reveal the complete cardiac cycle of the heart. Specialists use these studies to evaluate the mechanical function of the heart. Because the evaluation of the structures of the heart using cardiac CT has to be made over specific areas of the images, it is very useful to carry out some segmentation task at first.

Generally speaking, medical image segmentation is a prerequisite for many high-level tasks such as image analysis, computer-assisted diagnosis, geometric modeling of anatomical structures, or the construction of bio-mechanical models used for surgery simulation[2]. During decades, several algorithms for image segmentation in the field of medical application have been developed[3-6]. Many of them solved the problem by using statistical models[7-8], such as Markov random field[9], expectation maximization algorithm[10], and Bayesian discriminant functions [11-12], which use statistical information for pixel classification.

Another set of approaches are the so called deformable models. They consist of an initial instance that can be updated according to a set of forces in the neighborhood of a point. The shape is represented by a specific quantity of points describing the object contours in the image. These points are called landmarks and consist of the coordinates of the shape in the 2D or 3D space. The main advantage of these techniques is that they are capable of accommodating the common variability of biological structures. Active contour models, "Snakes" being the most popular deformable models, were proposed by Kass[13] et al., and consist of a framework that can delineate an object from an image. The method is based on the minimization of an energy associated to the current edge. It assumes that the energy is minimal when the "snake" is at the contour position. Some years later, Cootes et al. proposed a new method of models that can

Optics, Photonics, and Digital Technologies for Multimedia Applications II, edited by
Peter Schelkens, Touradj Ebrahimi, Gabriel Cristóbal, Frédéric Truchetet, Pasi Saarikko,
Proc. of SPIE Vol. 8436, 84361E · © 2012 SPIE · CCC code: 0277-786X/12/$18 · doi: 10.1117/12.922856

constrain the specific range of a training set. They called them "Active Shape Models" or "Smart Snakes"[14-15], and these methods have been employed by researches in modeling 2D and 3D structures in medical images[16-20].

Our goal is to extent 3D active shape models to represent time-series of 3D cardiac CT images. Segmentation of time-series images has been outlined for researches to solve different kinds of problems[21-22]. The most common applications of temporal shape modeling are given for cardiac image segmentation[23-24]. Montagnat[2] et al., attempt to model 4D objects using temporal constraints, they build a geometrical model based on the trajectory of corresponding vertices of the time-series represented by "simplex" meshes. Classical Newtonian law of motion is then used to describe the evolution of all vertices.

We propose an Active Shape Model-based segmentation method in which the time model statistics and gray level information are obtained from the training set in order to optimize the image search, i.e., the position of each landmark is updated taking into account not only the gray level information, such as the original model works, but also the time model characteristics. The rest of the paper is organized as follows. Section 2 presents a general description of active shape models. In section 3, we survey our method. Section 4 and 5 describe results and conclusion, respectively.

2. STATISTICAL MODELS OF SHAPE

Active shape models have demonstrated being a powerful segmentation tool for medical applications. The key point of this method is that instances of the models can only deform in ways found in the training set[14]. As a requisite for ASM algorithms, a set of shapes represented by *n* points in the spatial domain must exist.

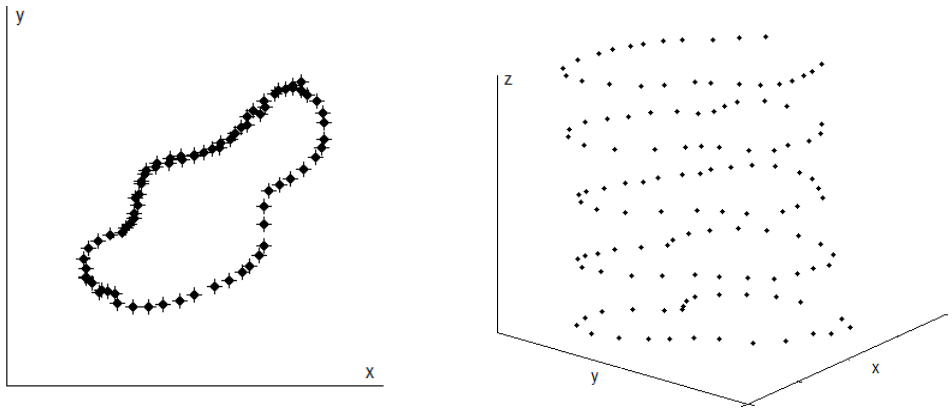

Figure 1. Landmarks in 2D and 3D spaces

When working with ASM, we can identify two main processes: the first of them is to capture the statistics of a training set by building a point distribution model and a gray level model for each landmark. The second process corresponds to the application of the models computed for the new image segmentation.

2.1 Point Distribution Model

In the 2D space (see figure 1), each shape S_i (with $i = 1, 2... N$) is a vector consisting of the concatenation of the coordinates of each landmark:

$$S_i = (x_0, y_0, x_1, y_1, ..., x_{n-1}, y_{n-1})^T \quad (1)$$

The first step is the aligning process of the training set to a mean shape that must be chosen from the contour samples. The most typical aligning method in 2D is the Generalized Procrustes Analysis – GPA[25]. Cootes et al., proposed a modified version of the GPA for 2D shapes that attempts to minimize a weighted error function with four unknown parameters:

$$E = (S_2 - MS_1 - T)^T W (S_2 - MS_1 - T) \quad (2)$$

where S_2 represents the mean shape and S_1 the one to be aligned; M is the transformation matrix that contains the s scale and θ rotation parameters; T represents the (tx, ty) translation incognita and W is a matrix with individual weight for each landmark. The step is repeated for all the shapes of the training set. A new mean shape is then calculated from the aligned samples X_i:

$$\overline{S} = \frac{1}{N}\sum_i X_i \tag{3}$$

Representation of shapes is quite similar for 3D spaces. Each landmark in this case is composed of three coordinates (x, y, z) and the shape vector is built in the same way:

$$S_i = (x_0, y_0, z_0, x_1, y_1, z_1, ..., x_{n-1}, y_{n-1}, z_{n-1})^T \tag{4}$$

It can be seen that each shape has a dimension of 2nd and 3rd orders for data in two-dimensional and three-dimensional spaces, respectively. Nonetheless, the aligning process in the 3D space is much more complicated. Here, several 3D images registering approaches can be used[26-27]. Hill et al. used the same minimization method depicted by equation (2), but for 3D objects. The problem in using this method is that the resulting equations are not linear and there are more unknown variables. They found the solution by considering several approximations to reduce the problem to a linear system, whose parameters can be calculated using conventional matrix methods. Once the mean shape is calculated, the next step is to compute the covariance of the data:

$$C = \frac{1}{N-1}\sum_{i=1}^{N}(S_i - \overline{S})(S_i - \overline{S})^T \tag{5}$$

Principal Component Analysis is finally applied in order to find all the parameters necessary to assemble the Point Distribution Model (PDM) of the data. This is carried out by computing the eigenvectors e_i and eigenvalues λ_i from the covariance matrix C. In this analysis, the principal modes of variation for each point are obtained. Since PCA reduces dimensionality of the data, only t eigenvectors corresponding to the higher eigenvalues are selected. Finally, the PDM is written as:

$$S = \overline{S} + Pb \tag{6}$$

where P is a matrix whose columns are the set of t eigenvectors given by the higher eigenvalues and b is a weight vector that can vary from $-3(\lambda_i)^{1/2}$ to $3(\lambda_i)^{1/2}$ as Cootes[14] proposed. New shapes are generated with different values of b.

2.2 Gray level profile model

This is the second part in the construction of the training set statistical models. Because PDMs are used for image search and segmentation, a model of the gray level information in the neighborhood of each landmark in the image that contains the shape is required. As shapes are described by points enclosing a contour, gray level profiles normal to each point are recommended for the modeling of the edges.

Having computed the gray level profile for each landmark, the next step is to obtain the first and second moments by calculating the mean and covariance matrix from the training set. Depending on the application, either the gray profile or its normalized derivative can be employed. Using the second characteristic (derivate of the gray profile) can be advantageous because it avoids the problem of different contrast in the images, what is very common in medical imaging, but at the same time it can be affected by noise. In the next section, we give more details of the method.

2.3 Active Search

This is the part where the models are addressed to segment new images. The active search starts by putting an initial instance near the object that will be segmented. Since ASM is a local method, we must ensure that the initialization is good enough to reach a solution. For this task, several algorithms have been proposed by researches in multiple applications[16, 28]. For both 3D and 2D shapes, the next step is to look for the strongest edge in the normal direction of the points in order to find a better position for each initial landmark. For this purpose, there must be an objective

function that gives the minimal value when it is evaluated on this edge profile. The most common used objective function is the Mahalanobis distance, though it has the problem that we have to invert covariance matrices. When there are not enough training samples, as is the case of medical applications, the covariance matrices are generally singular what makes impossible to use conventional methods to find their inverses.

When new positions for the landmarks are found, an aligning process must be computed to adjust the shape. Pose parameters (rotation, translation and scaling) are then obtained and used to calculate final deformations or shape parameters that move the current estimate to the new position. The process is iterative and it continues until reaching a specific number of iterations. Equations and mathematical formulation for this task are well explained by Cootes[14] for 2D images and by Hill[29] for 3D objects.

3. PROPOSED ASM-BASED METHOD FOR 4D OBJECTS (3D + TIME)

In this section, we outline the proposed solution to address the segmentation problem of three-dimensional structures that change with the time. The most common cases of this problem are the 4D cardiac CT images which are the objective of this work. It is known that three-dimensional images in medical applications are formed by a specific number of slices or 2D images. We assume that there is a set of time series of 3D objects previously segmented. They are represented by a set of points over each slice and describe the contour of the structure to be trained. In our application, the data (the time series of cardiac CT) are composed by a total of ten volumes (see figure 2) and the shape corresponds to the contour of the left ventricle of the heart. The ten volumes describe the complete cardiac cycle of the heart from systole to diastole.

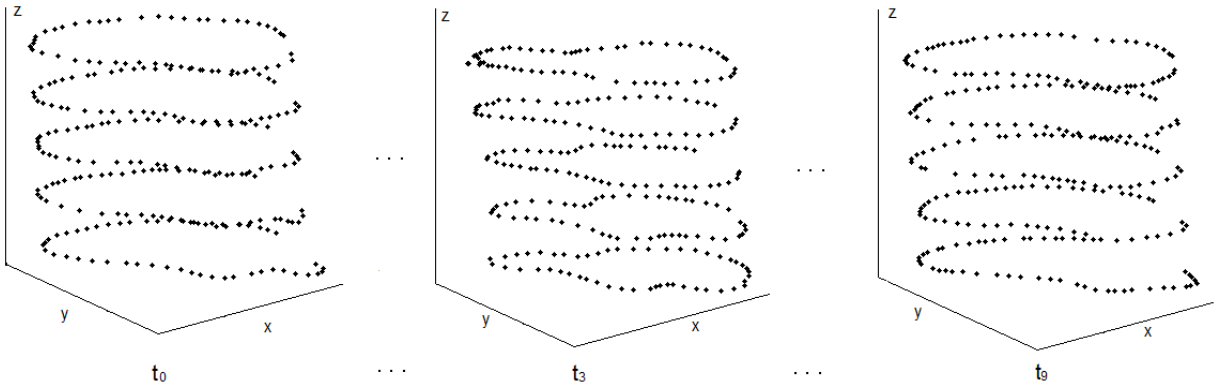

Figure 2. Landmarks for the time-series of 3D objects

We start our method by accommodating the points of the time sequence as a vector. Because the sequence of volumes is our "temporal shape", this vector must include all the landmarks for each volume. The concatenation begins with the first point of the time volume t_0 and ends with the last point of the time volume t_9. The mathematical representation of each temporal shape is as follow:

$$S_i = (x_{0t_0}, y_{0t_0}, z_{0t_0}, x_{1t_0}, y_{1t_0}, z_{1t_0}, \ldots, x_{(n-1)t_0}, y_{(n-1)t_0}, z_{(n-1)t_0}, \ldots, x_{0t_9}, y_{0t_9}, z_{0t_9}, x_{1t_9}, y_{1t_9}, z_{1t_9}, \ldots, x_{(n-1)t_9}, y_{(n-1)t_9}, z_{(n-1)t_9})^T \quad (7)$$

where $(x_{nt_k}, y_{nt_k}, z_{nt_k})$ is the coordinate of the point n in the time t_k. As it can be seen, the resulting vector that represents the time-series is of 30th dimension. The following steps for the training process are very similar. It is noticed that the points are in a three-dimensional space which implies that pose parameters must be calculated in 3D. Having organized the training vectors, we choose one of them as the initial mean temporal shape; the rest are aligned by using the approach described by Hill[29].

We assume that all the volumes of the time-series have the same quantity of points and the segmented shapes inside the volumes occupy the same number of slices. From the set of aligned vectors, the new mean temporal shape must be obtained. The aligning of shapes is an iterative process which is executed for a finite number of iterations or until the mean shape does not suffer modifications from one iteration to other. As depicted in section 2, the mean of the time-sequence is calculated by using equation (3).

Continuing with the training, covariance matrix and PCA of the aligned vectors are computed to finally build the Point Distribution Model. This model is not able to capture the complete variability of the cardiac CT structures if we do not have enough training samples.

3.1 Computing the gray level statistics

In the previous section we mentioned that for the active search in the segmentation process, we need a gray level model for every landmark's profile. Assume that P_{k,t_n} is the *k-th* landmark for the *n-th* volume of the time-series. A profile normal to the surface in this point can be defined as:

$$g_{k,t_n} = \{(P-l)_{k,t_n},(P-l+1)_{k,t_n},...,P_{k,t_n},...,(P+l-1)_{k,t_n},(P+l)_{k,t_n}\} \tag{8}$$

where l defines the extremes of the profile to each side of the principal point and follows a normal direction to the landmark. The size of the profile must be chosen as well. Most of the time, applications have to deal with the problems of contrast in the images and poor definition of edges, we choose to work with the normalized derivative dg_{k,t_n} of the profile. The mean profile and its mean normalized derivative for the *k-th* landmark are calculated from the samples of the training set as:

$$\bar{g}_{k,t_n} = \frac{1}{N}\sum_{i=1}^{N} g_{ik,t_n} \quad , \quad \overline{dg}_{k,t_n} = \frac{1}{N}\sum_{n=1}^{N} dg_{ik,t_n} \tag{9}$$

Finally, the gray model is completed with the covariance matrix of the profile for each landmark of the time-sequence vector, including the profile:

$$Y_{k,t_n} = \frac{1}{N-1}\sum_{i=1}^{N}(g_{ik,t_n} - \bar{g}_{k,t_n})(g_{ik,t_n} - \bar{g}_{k,t_n})^T \ , \tag{10}$$

and its normalized derivative:

$$dY_{k,t_n} = \frac{1}{N-1}\sum_{i=1}^{N}(dg_{ik,t_n} - \overline{dg}_{k,t_n})(dg_{ik,t_n} - \overline{dg}_{k,t_n})^T \tag{11}$$

where T represents the transpose of the vector and N the number of training samples.

3.2 Construction of the time model

The main problem we are dealing with on this project is to make a representation of 3D objects that are changing their structures periodically, as is the case of the heart. It is well known that this organ is constantly moving and its mechanical behavior can be evaluated using some techniques like computed tomography imaging. In this sense, 4D cardiac CT studies provide heart images at each period of time or cardiac cycle. Reviewing equation (7), the existence of corresponding points in each volume of the temporal shape is obvious, i.e., a landmark must be included in each volume of the time-sequence. For example, it is found from equation (7) that points $(x_{0t_0}, y_{0t_0}, z_{0t_0})$,…, $(x_{0t_9}, y_{0t_9}, z_{0t_9})$ are the same but distributed in the ten volumes of the time-series. Looking this from an image analysis point of view, we can observe that each point in the sequence describes a trajectory; because images code spatial information of objects, the trajectory depicted by each point is governed by changes of positions or coordinates along the volumes of the series.

Now, it is possible to construct a time model that describes the behavior of each point of the shape when it is seen from one volume to other. Here, we follow the same criteria as the gray level model because of the variability that exhibits the

structures of the heart for different patients. Assuming the same nomenclature as the last case, we have that P_{k,t_n} represents the *k-th* landmark for the *n-th* volume of the time-series with coordinates ($x_{kt_n}, y_{k\,t_n}, z_{k\,t_n}$). The vector describing the mentioned trajectory is the concatenation of the points in this way:

$$V_k = (P_{k,t_0}, P_{k,t_1}, P_{k,t_2}, P_{k,t_3}, P_{k,t_4}, P_{k,t_5}, P_{k,t_6}, P_{k,t_7}, P_{k,t_8}, P_{k,t_9}) \tag{12}$$

where t_n indicates a particular volume of the sequence. In general, cardiac CT images taken from different patients and equipments present a varying size of the structures of the heart. Normalizing the vector allows us to remove the scaling factor among them. This is done by using an isomorphic scaling:

$$T_k = \frac{V_k}{\|V_k\|} \tag{13}$$

where $\|\cdot\|$ is the Euclidean norm of the vector. The mean normalized trajectory vector is calculated:

$$\overline{T}_k = \frac{1}{N}\sum_{i=1}^{N} T_{ik} \tag{14}$$

with *N* being the number of volumes that contains the time-sequence. Finally, the covariance matrix of the trajectory for each landmark is obtained:

$$CV_k = \frac{1}{N-1}\sum_{i=1}^{N} (T_{ik} - \overline{T}_k)(T_{ik} - \overline{T}_k)^T \tag{15}$$

The time model is kept as the first and second order trajectory statistic described by each landmark in the temporal shapes of the training set.

3.3 Objective function in the active search

We have said that once the models have been constructed, the algorithm is ready to find new examples of shapes in the sample images. In the active search used for image segmentation, it is necessary to define an objective function that determines the best positions where the landmarks of the initial shape have to be moved in order to better fit the data. When working with medical images, it is very common to find problems related to the contrast and noise what make difficult to carry out some tasks such as segmentation.

ASM algorithms start the process of segmentation by putting, manually or in automatic way, an initial instance as closed as possible to the structure to be segmented. Each landmark is moved to a better position in the normal direction by minimizing the objective function. Giving the differences of contrast, the noise and the temporal behavior of 4D cardiac CT images, we proposed a weighted sum of Mahalanobis distances of the gray profile, its normalized derivative and the model time as objective functions for each point:

$$f_{P_k i} = w_1(g_{P_k i} - \overline{g}_k)Y_{P_k}^{-1}(g_{P_k i} - \overline{dg}_{P_k})^T + w_2(dg_{P_k i} - \overline{dg}_{P_k})dY_{P_k}^{-1}(dg_{P_k i} - \overline{dg}_{P_k})^T + w_3(T_{P_k i} - \overline{T}_{P_k})CV_{P_k}^{-1}(T_{P_k i} - \overline{T}_{P_k})^T \tag{16}$$

where w_m (m = *1,2,3*) is the assigned weight for each part of the objective function, P_k (k = *1, 2, ..., n*) indicates the respective landmark and *i* represents a specific position of the landmark P_k along its normal profile. Hence, the new positions of the points are finally chosen according to the minimal value obtained for the function f_{P_k} evaluated in the normal direction of P_k.

When new positions are determined, the process continues with the alignment of the initial shape and the one defined for the new landmarks. Here, angle of rotation, translation vector and a scaling factor are computed. These variables correspond to pose parameters of the data. New modifications are still necessary to adjust the data in order to reach the found solution; shape parameters are subsequently obtained in terms of the transformation matrix (rotation, translation and scaling) and eigenvectors calculated in the training stage. The final shape is calculated from the initial one by using

the pose and shape parameters. Since it is an iterative process, the final result becomes the initial shape for the next iteration. A complete description of the adjusting mechanism can be reviewed[14].

4. EXPERIMENTS AND RESULTS

We evaluated our method for several time-series of cardiac CT images. The structure used for the segmentation was the left ventricle of the heart from an axial view. The initial instance for each test corresponds to the mean shape of the training and it is put manually onto the time-sequence. Figure 3 illustrates four slices of the first three volumes of the time-series used to test the algorithm showing the left ventricle in four-chamber axial view.

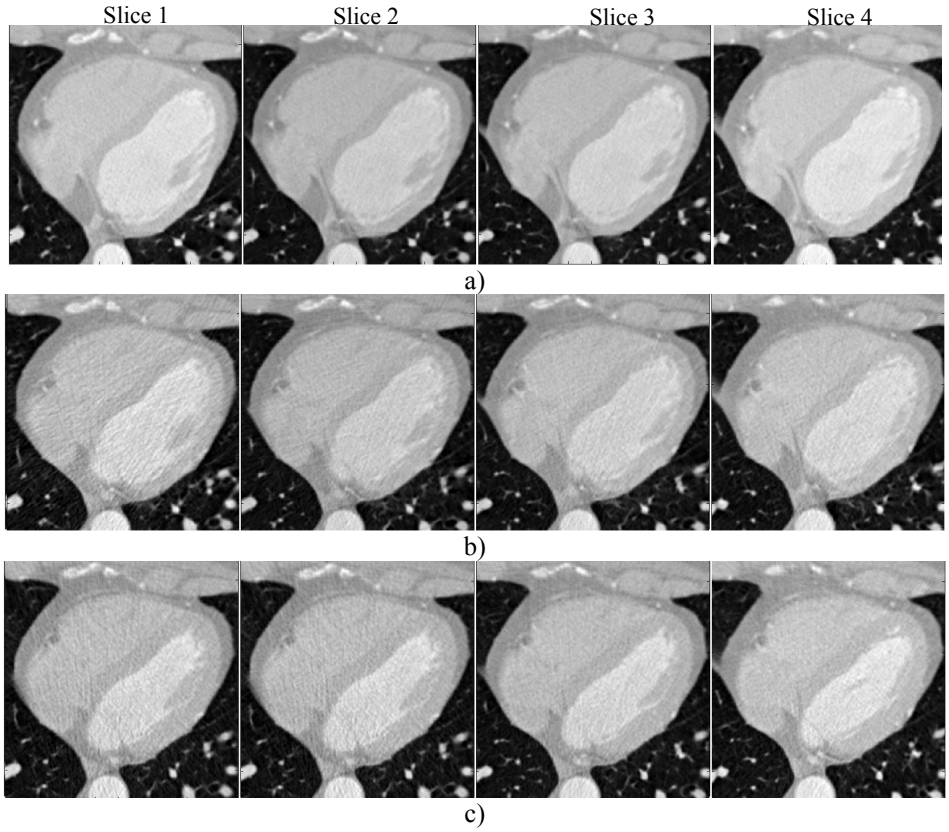

Figure 3. Four slices of the time-series used to test the algorithm, a) Volume 1; b) Volume 2 and c) Volume 3

As can be seen from the last figure, the left ventricle of the heart exhibits a great variability from one volume to the next in the images of the time-series. Depending on several characteristics of patients like age, gender or some cardiac diseases, the shape of this structure can vary considerably as well.

4.1 Performance Metric

The segmentation algorithm is computed for images that were not used in the training process. We carried out visual and quantitative performance evaluations of the automatic segmentation for each sample. For the quantitative assessment, we used a metric given by the mean Euclidian distance per point which is an easy but effective method that can measure the mean separation of each point of the shapes. Given two points P_1 and P_2, the Euclidian distance between them can be calculated as:

$$d_{P_1,P_2} = \sqrt{\sum_{i=1}^{N}(P_{1i} - P_{2i})^2} \tag{17}$$

where N is the size of P_1 and P_2 (N = 3 for volumes); d corresponds to the desired distance.

In our evaluation, we then calculate the distance between the automatic (for the first and final iterations) and manual segmentations of the temporal shapes. In this project, results are given for eight 4D cardiac CT images. In table 1, the obtained performance for all the samples is summarized.

Table 1. Characteristics of the samples and Euclidean distance between the automatic and manual segmentations.

Sample	Volumes of the Time-Series	Slices per Volume	Slices Segmented	Mean Euclidean Distance/point of the Initial Instance	Mean Euclidean Distance/point of the Final Result
Time-Series 1	10	80	5	5.45735	5.19752
Time-Series 2	10	145	5	4.47716	4.08912
Time-Series 3	10	66	5	3.95231	3.58310
Time-Series 4	10	66	5	4.12130	3.74103
Time-Series 5	10	76	5	2.95268	2.71527
Time-Series 6	10	81	5	3.60540	3.11042
Time-Series 7	10	130	5	3.59310	3.44656
Time-Series 8	10	136	5	4.93335	4.25979

Figures 4 and 5 illustrate the starting temporal shape and the final segmentation for the 4D cardiac CT image of figure 3. The initialization is made manually by putting the mean temporal shape resulting from the training near the object.

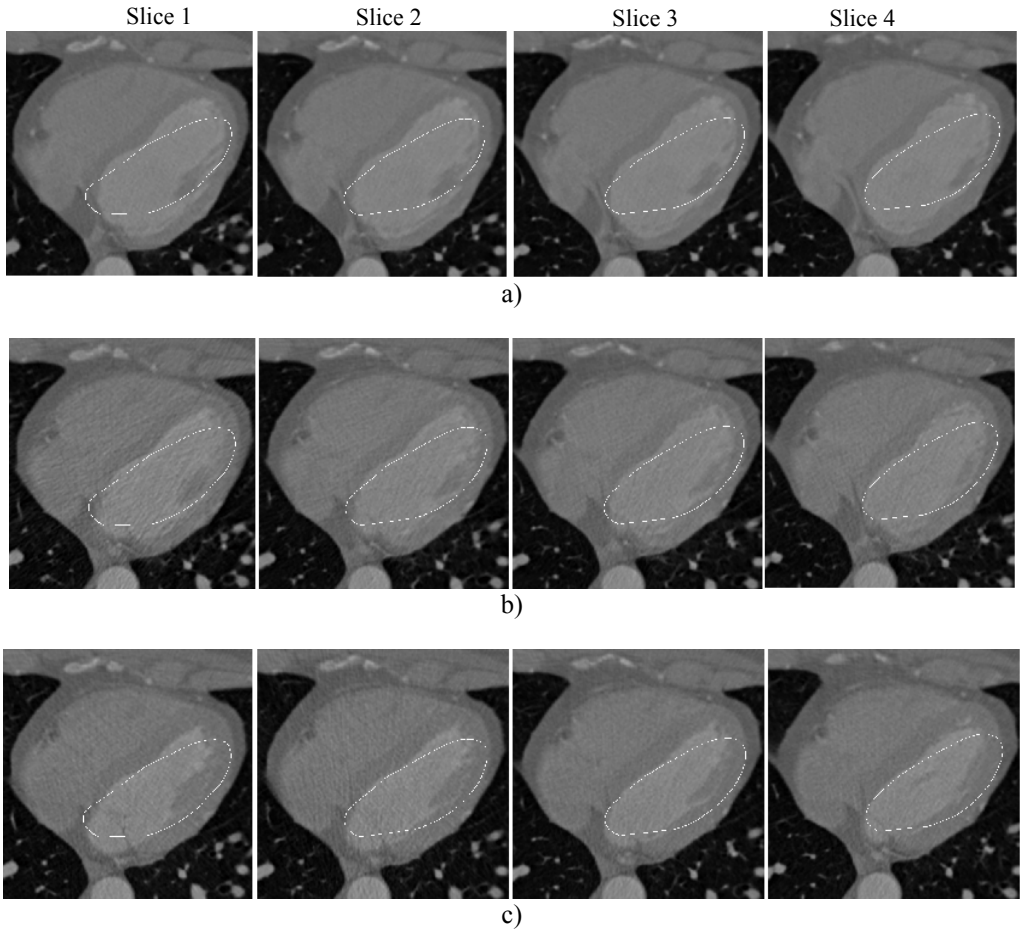

Figure 4. Initial segmentation of the time-series of figure 3, a) Volume 1; b) Volume 2 and c) Volume 3

Table 1 shows that all the time series used for the evaluation of the algorithm do not have the same number of slices what means that they have different spatial resolutions along the z coordinate. Because the method implies that each temporal shape must contain the same number of slices, we must either make an interpolation or subsampling of the data with the aim of getting similar shapes.

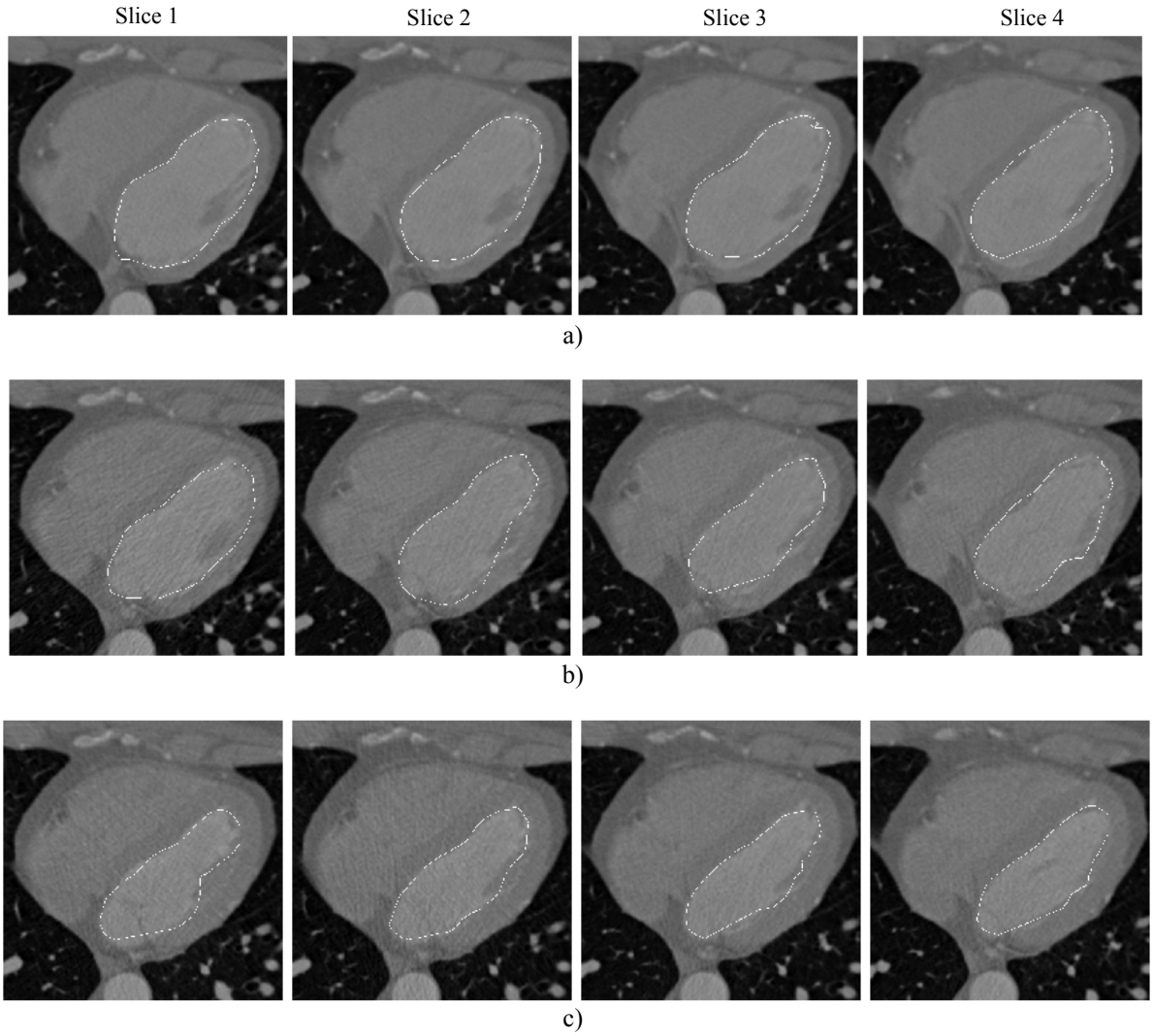

Figure 5. Final segmentation of the time-series shown in figure 3, a) Volume 1; b) Volume 2 and c) Volume 3

4.2 Discussion

As reflected in table 1, the ASM proposed model presents good results for segmentation of cardiac CT time-series images. The obtained performance is improved when the quantity of training samples is increased. What is expressed in this table is the mean distance for each volume's voxel in the time-series with respect to the manual segmentation. Figures 3 to 5 correspond to the first time-series of table 1, which is useful to make comparisons between the visual and the quantitative performance. For this project we used 70 times series of cardiac CT for the PDM construction. This results in 43 eigenvectors that encode the complete variability of the left ventricle of the heart.

For each slice we used 50 points around the contour of the left ventricle in an axial view. Since the objective of the proposed approach is to adapt it to optic flow estimation algorithms for mechanical evaluation of the heart, we only selected 5 slices per volume. This means that the time-series is represented by 2500 points. With the purpose of closing the contour in the images for visual representation, we used an algorithm that makes an interpolation among the points.

In order to reach the final solution, at least 40 iterations were necessary. It is observed in figure 5 that some visual errors are present in the final segmentation. Some of these problems can be solved by taking more landmarks for the contour.

There is no method to choose the weight parameters for the objective function in the active search. These are selected experimentally. Good results were obtained for $w_1 = 0.3$, $w_2 = 0.7$ *and* $w_3 = 1$. The idea of using weight is to compensate common problems normally presented on images. Even though working with the derivative function of the profiles is a good method to deal with contrast problems, it has the disadvantage that is very sensitive to image noise. However, when there are several edges very closed each other, the derivative function of the profiles can produce errors in the segmentation.

5. CONCLUSIONS

We have built an ASM-based method for segmentation of 4D cardiac computed tomography images. The goal of the project is to address automatic segmentations of the left ventricle and the structures around it, which is helpful to evaluate the heart mechanical functions. The detected behavior allows the doctor to take decisions about better procedures related to patient's health. Because manual segmentations are always tedious and time consuming, automatic algorithms are always a good alternative.

The proposed approach presents good results when enough training samples are used. This is a disadvantage of ASM models due to the fact that the quantity of eigenvectors defines how many deformations the shape in the active search can suffer. On the other hand, the initialization must be good enough to reach the final solution. We opted for manual initialization although automatic methods can be used as well.

The method was validated with eight time-series of cardiac CT images. The algorithm was compared with manual segmentations by calculating the mean Euclidean distance of each point. From the experimental findings, we realized that using a combination of the gray profile statistics, their derivative function and the time model as objective function, improves significantly the performance of the segmentation.

ACKNOWLEDGMENTS

This work has been sponsored by the following UNAM grant: PAPIIT IN113611 and CONACYT México. Barba-J thanks COLCIENCIAS Colombia for financial support in the project.

REFERENCES

[1] Matthew, J., Budoff and Jerold S., S., [Cardiac CT Imaging, Diagnosis of Cardiovascular Disease], Springer-Verlag, London, 27-39 (2006).

[2] Johan Montagnat, Hervé Delingette, "4D deformable models with temporal constraints: application to 4D cardiac image segmentation," Medical Image Analysis 9, 87-100 (2005).

[3] Aboutanos, G.B. and Dawant, B.M., "Automatic brain segmentation and validation: image-based versus atlas-based deformable models," Proc. Medical Imaging SPIE 3034, 299–310 (1997).

[4] Ashton, E.A., Berg, M.J., Parker, K.J., Weisberg, J., Chen, C.W., and Ketonen, L., "Segmentation and feature extraction techniques, with applications to MRI head studies," Mag. Res. Med. 33, 670–677 (1995).

[5] Bloomgarden, D.C., Fayad, Z.A., Ferrari, V.A., Chin, B., Sutton, M.G.S.J. and Axel, L., "Global cardiac function using fast breath-hold MRI: Validation of new acquisition and analysis techniques," Magnetic Resonance in Medicine 37, 683–692 (1997).

[6] Bae, K.T., Giger, M.L., Chen, C., and Kahn, C.E., "Automatic segmentation of liver structure in CT images," Med. Phys. 20, 71–78 (1993).

[7] Tianhu, L. and Wilfred Sewchand, "Statistical approach to X-Ray CT imaging and its applications in image analysis – part II: A new stochastic model-based image segmentation technique for X-Ray CT image," IEEE T. Med. Imag. 11(1), 62–69 (1992).

[8] McInerney, T. and Terzopoulos, D., "A dynamic finite element surface model for segmentation and tracking in multidimensional medical images with application to cardiac 4D image analysis," Comput. Med. Im. Graph. 19, 69–83 (1995).
[9] Held, K., Kops, E.R., Krause, B.J., Wells, W.M. III., Kikinis, R., Muller-Gartner, H.-W., "Markov random field segmentation of brain MR images," IEEE T. Med. Imag. 16(6), 878-886 (1997).
[10] Lorenzo-Valdéz, M., Sanchez-Ortis, G.I., Mohiaddin, R., and Rueckert, D., "Segmentation of 4d cardiac MR images using a probabilistic atlas and the EM algorithm," Proc. MICCAI 2878, 440–450 (2005).
[11] Hurn, M.A., Mardia, K.V., Hainsworth, T.J., Kirkbride, J., and Berry, E., "Bayesian fused classification of medical images," IEEE T. Med. Imag. 15, 850–858 (1996).
[12] Laidlaw, D.H., Fleischer, K.W., and Barr, A.H., "Partial-volume bayesian classification of material mixtures in MR volume data using voxel histograms," IEEE T. Med. Imag. 17, 98–107 (1998).
[13] Kass, M., Witkin, A., and Terzopoulos, D., "Snakes: Active contour models," Int. J. Comp. Vision 1, 321–331 (1988).
[14] Cootes, T.F., Taylor, C.J., Cooper, D.H., and Graham, J., "Active shape models - their training and application," Computer Vision and Image Understanding 61(1), 38–59 (1995).
[15] Cootes, T.F., Hill, A., Taylor, C.J. and Haslam, J., "The use of active shape models for locating structures in medical images," Proc. IPMI 1993, 33–47 (1993).
[16] Cosio, F.A., "Automatic initialization of an active shape model of the prostate," Medical Image Analysis 12(4), 469–483 (2008).
[17] Mitchell, S.C., Bosch, J.G., Lelieveldt, B.P.F., van der Geest, R.J., Reiber, J.H.C. and Sonka, M., "3-D active appearance models: segmentation of cardiac MR and ultrasound images," IEEE Transactions on Medical Imaging 21(9), 1167–1178 (2002).
[18] Van Assen, H. C., Danilouchkine, M. G., Frangi, A. F., Ordás, S., Westenberg, J. J. M., Reiber, J. H. C., Lelieveldt, B. P. F., "SPASM: A 3D-ASM for segmentation of sparse and arbitrarily oriented cardiac MRI data," Medical Image Analysis 10, 286–303 (2006).
[19] Tobias Heimann, Hans-Peter Meinzer, "Statistical shape models for 3D medical image segmentation: A review," Medical Image Analysis 13, 543-563 (2009).
[20] Frangi Alejandro, Daniel Rueckert, Julia Schnabel and Wiro Niessen, "Automatic 3D ASM Construction via Atlas-Based Landmarking and Volumetric Elastic Registration," Proc. IPMI 2082, 78-91 (2001).
[21] Ghassan, H. and Tomas Gustavsoon, "Deformable spatio-temporal shape models: extending active shape models to 2D + time," Image and Vision Computing 22, 461-470 (2004).
[22] Timo Kohlberger, Daniel Cremers, Mikael Rousson, Ramamani Ramaraj and Gareth Funka-Lea, "4D Shape Priors for a Level Set Segmentation of the Left Myocardium in SPECT Sequences," Proc. MICCAI 4190, 92-100 (2006).
[23] Chandrashekara, R., Rao, A., Sanchez-Ortiz, G. I. and Ruecker, D., "Construction of a statistical model for cardiac motion analysis using nonrigid image registration," Proc. IPMI 2003, 599-610 (2003).
[24] Debreuve, E., Barlaud, M., Aubert, G., Laurette, "Space-time segmentation using level set active contours applied to myocardial gated SPECT," IEEE Transactions on Medical Imaging 20(7), 643–659 (2001).
[25] Dryden, I. L. and Mardia, K. V., [Statistical Shape Analysis], Jhon Wiley & Sons, New York, 83-107 (1998).
[26] Paul, J. B. and Neil, D. M., "A Method for Registering of 3-D Shapes," IEEE Transactions on Pattern Recognition and Machine Intelligence 14(2), 239-256 (1992).
[27] Chandrashekara, R., Rao, A., Sanchez-Ortiz, G.I., Mohiaddin, R.H., Rueckert, D., "Construction of a statistical model for cardiac motion analysis using nonrigid image registration," Proc. Taylor C. J. A. N. Information Processing in Medical Imaging 2732, 599–610 (2003).
[28] Karim, L. and Guang-Zhong Yang, "Optimal Feature Point Selection and Automatic Initialization in Active Shape Model Search," Proc. MICCAI 5241, 434–441 (2008).
[29] Hill, A., Thornham and Taylor, C. J., "Model –Based Interpretation of 3D Medical Images," Proc. 4th British Machine Vision Conference 1993, 339-348 (1993).